SSRG International Journal of Electronics and Communication Engineering
ISSN: 2348-8549/ https://doi.org/10.14445/23488549/IJECE-V11I7P106

Volume 11 Issue 7, 53-64, July 2024
© 2024 Seventh Sense Research Group®

Original Article

Optimization of the Highly Efficient GaAs Solar Cell

Jhilirani Nayak[1], Priyabrata Pattanaik[2], Dilip Kumar Mishra[3]

[1,2,3]*Faculty of Engineering and Technology (ITER), Siksha 'O' Anusandhan Deemed to be University, Odisha, India.*

[1]*Corresponding Author : jhiliraninayak@soa.ac.in*

Received: 05 May 2024 Revised: 05 June 2024 Accepted: 04 July 2024 Published: 27 July 2024

Abstract *- The paper comprehensively explores and investigates the effect of each layer of the implemented Gallium Arsenide (GaAs) solar cell, introducing an Aluminum Gallium Arsenide (AlGaAs) window layer. The device performance with respect to the critical parameters is a major concern. This strategic utilization of the AlGaAs window layer and other layers provides their effect on the key parameters of the device. The study primarily centers on the assessment of the solar cell's performance, with a particular focus on key metrics such as Short-Circuit Current (Isc), Fill Factor (FF) and Open-Circuit Voltage (Voc). The analysis encompasses an exhaustive exploration of several critical parameters, encompassing window layer thickness, window layer concentration, and radiative recombination coefficient. To achieve the research objectives, an optimization approach is pursued, commencing with the initial refinement of the solar cell device, followed by a subsequent optimization phase aimed at enhancing efficiency under the AM 1.5 spectrum, resulting in an impressive efficiency improvement of up to 34.28% (1 sun). This marked enhancement surpasses prior outcomes reported in the existing literature.*

Keywords *- AlGaAs window layer, Absorber layer, Energy band gap, Mole fraction, Optimization, Radiative recombination.*

1. Introduction

Solar cells are electronic devices that are used to produce electrical energy from solar radiation. This device works on the basis of the photovoltaic effect [1]. The photovoltaic effect is an induced potential difference due to the generated electron-hole pair in a semiconductor [2-4]. The purpose of photovoltaic cells is to produce electricity from incident solar radiation. The efficiency of Photovoltaic (PV) cells is contingent upon several crucial factors, including the energy band gap and carrier charge recombination mechanisms. These intrinsic limitations in PV cell performance are to optimize the maximum Open-Circuit Voltage (V_{OC}) [5]. The attainment of high efficiency in silicon (Si) photovoltaic cells at 25.6% and gallium arsenide (GaAs) solar cells at 26.4% is impeded by the suboptimal arrangement of radiation trapping mechanisms and the presence of parasitic losses in their design. Preferably, people are seeking a solar cell that provides enhanced performance while being more cost-effective [1]. So, thin film technologies have been developed [6]. Till now, thin film technology with Gallium arsenide material has been used widely because of its higher charge carrier mobility, direct bandgap and higher absorption coefficient. Using AlGaAs as a window layer and a BSF layer enhances the efficiency [7]. Considering the demanding temperature conditions, Gallium arsenide solar cells are the standard ones [8].

In this study, the performance enhancement of an n+-type AlGaAs window-layered GaAs solar cell has been investigated. This novel design employs a sandwich structure comprising a GaAs solar cell situated between an AlGaAs window layer at a mole fraction of 0.4 and an AlGaAs BSF layer. Incorporating the AlGaAs wide bandgap layer significantly enhances the efficiency of the cell. This achievement is due to less reflectance, thereby boosting voltage output and simultaneously augmenting photon absorption. To optimize performance, the dimensions and dopant concentrations of the various layers within the cell were adjusted systematically. Our analysis also pertains to the evaluation of radiative recombination variations. To comprehensively assess the proposed solar cell's performance, extensive simulations were conducted using the SCAPS device simulator [9].

2. Simulation Methodology

The 3-D view of a new n^+-type AlGaAs window layer GaAs photovoltaic device is presented in Figure 1. The structure of the proposed device consists of back contact/silicon-buffer/P+-GaAs/AlGaAs back surface field/P-GaAs /n-GaAs /n+-AlGaAs /front contact. The AlGaAs alloy contains 41% of the aluminum composition. The window layer and emitter layer are doped with pentavalent impurities, and the base layer is doped with trivalent impurities**.** A back surface field of AlGaAs and a silicon buffer has been used. The presence of AlGaAs enhances the current due to the short circuit and efficiency of the device. Similarly, the buffer layer is used to provide stability and improvement in I_{sc} and η. Here, the window layer thickness is optimized for better efficiency.

This is an open access article under the CC BY-NC-ND license (http://creativecommons.org/licenses/by-nc-nd/4.0/)

AlGaAs window layer has gained popularity because of the wide band gap and large absorption coefficient. The proposed structure has been simulated using a SCAPS 1D device simulator, and the properties of the materials from the literature [10] are summarized in Table 1**.** The proposed device's characteristics are compared with the previously reported study [10] is given in Table 2**.** The simulation results deal with the study of device performance parameters with respect to mole fraction, different concentrations of window layer and radiative recombination coefficients.

A number of simulation tools, including ATLAS, PC1D, AFOR-HET, AMPS,wxAMPS and SCAPS-1D [12-17], are used for the investigation of device performance and feasibility. In the current study, the SCAPS software is employed to conduct simulations on photovoltaic cells utilizing GaAs absorbers. SCAPS software is a widely recognized tool for simulating the electrical characteristics and behavior of photovoltaic cells, making it an indispensable resource in the field of photovoltaics. Its foundation lies in a set of interconnected differential equations that precisely model carrier transport within semiconductor materials. These equations are grounded in the fundamental principles governing charge transport processes in semiconductors.

They are

(a) Equations based on the transport of carriers

$$J_n = -\frac{\mu_n n}{q}\frac{\partial E_{Fn}}{\partial x} \quad (1)$$

$$J_p = +\frac{\mu_p p}{q}\frac{\partial E_{Fp}}{\partial x} \quad (2)$$

(b) Continuity equation for charge carriers

$$-\frac{\partial J_n}{\partial x} - U_n + G = \frac{\partial n}{\partial t} \quad (3)$$

$$-\frac{\partial J_p}{\partial x} - U_p + G = \frac{\partial p}{\partial t} \quad (4)$$

and

(c) Boundary conditions of the device are solved by using the Poisson equation.

$$\frac{\partial}{\partial x}\left(\varepsilon_0 \varepsilon_r \frac{\partial \psi}{\partial x}\right) = -q(p - n + N_D^+ - N_A^- + \frac{\rho_{def}}{q}) \quad (5)$$

J_n and J_p are the notations for electron current density and hole current density, where as μ_n and μ_p represents the notations for mobility of electrons and holes. The electronic charge is represented by q and E_{Fn} and E_{Fp} represents the quasi-fermi energy levels for charge carriers. The recombination rate for electrons and holes is represented by $U_n$and U_p and G represents the electron-hole generation rate. ε_0, ε_r, ψ, n, N_D^+, p , N_A^- and ρ_{def} represent the absolute permittivity, relative permittivity, electrostatic potential, electron concentration, donor density, hole concentration, acceptor density, and charge density defects.

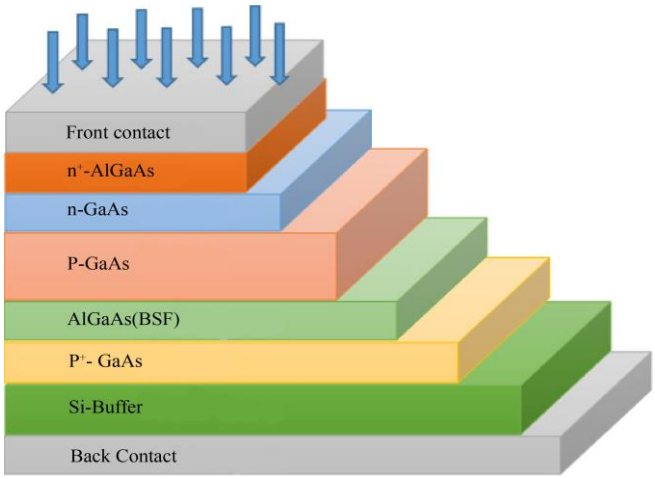

Fig. 1 A schematic device architecture of GaAs-based absorber solar cell (proposed)

3. Results and Discussion

This article's primary goal is the comprehensive investigation, analysis and optimization of photovoltaic device parameters. To establish a framework to design the device adhering to the highest efficiency, an optimization approach was employed. For the optimization process, the SCAPS-1D software tool is utilized. The optimization procedure, grounded in theoretical analysis, encompassed fine-tuning a spectrum of critical parameters, namely: (a) Thickness optimization in the n^+-type AlGaAs layer and GaAs absorber layer, (b) Refining carrier concentrations in the n^+-type AlGaAs layer and GaAs absorber layer,(c) Enhancing radiative recombination coefficient, (d) Optimization corresponding to number of suns and (e) Emitter layer thickness optimization. In the case of $Al_xGa_{1-x}As$ alloy, as Al partially replaces Ga in GaAs, its band gap increases, and the electron affinity decreases. As the mole fraction gradually rises from 0 to 1, the energy band gap also rises from 1.42eV to 2.16eV [18]. In this system, the bandgap used for $Al_xGa_{1-x}As$ is a direct bandgap at x=0.4. The compound semiconductor energy bandgap corresponding to the composition(x) is generally presented as

$$E_g = a + bx + cx^2 \quad [10]$$

For $Al_xGa_{1-x}As$ alloy, the energy band gap is given by

$$E_g = 1.424 + 1.247x(eV) \qquad x < 0.45 \quad [10]$$

$$E_g = 1.9 + 0.125x + 0.143x^2 \qquad x \geq 0.45 \quad [10]$$

The electron affinity is expressed as

$$\chi(x) = 4.07 - 1.1x(eV) \qquad x < 0.45 \quad [10]$$

$$\chi(x) = 3.64 - 0.14x(eV) \qquad x \geq 0.45 \quad [10]$$

Al alloying influences most of the physical properties of the device. The band gap variation of AlGaAs with respect to mole fraction is shown in Figure 2.

Table 1. List of material/device parameters

Parameters	Si	p^+-GaAs	p-GaAs
Thickness (µm)	1	0.5	2.0
Bandgap of Material (eV)	1.12	1.424	1.424
Electron Affinity (eV)	4.05	4.07	4.07
Dielectric Permittivity (ε_r)	11.8	12.9	12.9
CB Effective Density of State N_c($x10^{18}cm^{-3}$)	28	0.17	0.17
VB Effective Density of State N_v($x10^{18}cm^{-3}$)	10	10	10
Electron Thermal Velocity (cm s^{-1})	$2.3x10^5$	$4.4x10^5$	$4.4x10^5$
Hole Thermal Velocity (cm s^{-1})	$1.65x10^5$	$1.0x10^5$	$1.0x10^5$
Electron Mobility (cm^2 v^{-1} s^{-1})	$1.4x10^3$	$8.5x10^3$	$8.5x10^5$
Hole Mobility of Material (cm^2 v^{-1} s^{-1})	$4.5x10^2$	$3.7x10^2$	$3.7x10^2$
Donor/Acceptor Density, N_D/N_A (cm^{-3})	$1.0x10^{19}$	$1.0x10^{18}$	$1.0x10^{16}$
Absorption Coefficient (cm^{-1})	SCAPS file	SCAPS file	SCAPS file

Parameters	n-GaAs	AlGaAs	n+-AlGaAs
Thickness (µm)	0.1	0.5	0.02
Bnadgap of Material (eV)	1.424	1.86	1.86
Electron Affinity (eV)	4.07	3.74	3.74
Dielectric Permittivity (ε_r)	12.9	10.6	10.6
CB Effective Density of State N_c($x10^{18}cm^{-3}$)	0.17	80 $x10^{18}cm^{-3}$	80 $x10^{18}$
VB Effective Density of State N_v($x10^{18}cm^{-3}$)	10	10 $x10^{18}cm^{-3}$	10 $x10^{18}$
Electron Thermal Velocity (cm s^{-1})	4.4	$2.3x10^5$	$2.3x10^5$
Hole Thermal Velocity (cm s^{-1})	$1.0x10^5$	$1.40x10^5$	$1.4x10^5$
Electron Mobility (cm^2 v^{-1} s^{-1})	$8.5x10^3$	$2.12x10^2$	$2.12x10^5$
Hole Mobility (cm^2 v^{-1} s^{-1})	$3.7x10^2$	$1.26x10^2$	$1.26x10^2$
Donor/Acceptor Density, N_D/N_A (cm^{-3})	$1.0x10^{18}$	$1.0x10^{17}$	$2.0x10^{19}$
Absorption Coefficient (cm^{-1})	SCAPS file	SCAPS file	SCAPS file

Figure 2 illustrates the device performance characteristics as a function of mole fraction, ranging from 0 to 1. In Figures 2 (a) and (b), it is evident that both efficiency and short-circuit current density reach their peak values when x=0.4. This observed peak efficiency is due to the enhanced absorption of solar radiation within the visible portion of the electromagnetic spectrum. Additionally, Figures 2 (c) and (d) depict a decrease in the FF and V_{oc} with an increase in mole fraction.

3.1. The Effect of Window Layer and Absorber Layer Thickness

In the structured device, an AlGaAs window layer is strategically positioned as the top layer. This layer allows the transmission of incident light through it while facilitating the efficient collection and extraction of generated electrical charge carriers. Optimizing the thickness of the AlGaAs window layer enhances light absorption efficiency while concurrently mitigating carrier recombination losses. The potential difference due to the open-circuit of the AlGaAs window layer is chiefly governed by two key factors: The material's bandgap energy and the pn-junction built-in potential. The potential difference due to the open-circuit remains invariant at a precise value of 1.3104V due to the constant nature of the material's bandgap and induced built-in potential.

However, the AlGaAs window layer thickness exceeds 10µm, and a fall in the open-circuit voltage is observed, as depicted in Figure 3 (a). The photovoltaic device's Fill Factor (FF) is a measure of its efficiency and is determined by the open-circuit potential difference. As the open-circuit potential difference decreases, the fill factor also decreases. In the proposed device, the AlGaAs window layer is typically used to have a wider bandgap. This layer allows the incident light to be transmitted while minimizing the carrier recombination within the GaAs layer.

The increased thickness of the AlGaAs window layer affects the short circuit current, as illustrated in Figure 3 (b). The current attains its maximum value at a thickness of 5.5µm. After achieving the maximum value, there is a fall down. This fall down is because of the longer optical path for incident photons to travel before reaching the absorber layer.

This indicates that more photons are absorbed within the AlGaAs window layer itself rather than being transmitted to the absorber layer to generate electron-hole pairs. A significant enhancement in efficiency is observed in the Figure 3(c) due to the increase in thickness. A maximum value of 34.33% is achieved at a thickness of 5.5µm and then reduces due to the loss of photons and increase in series resistance. Absorber layer thickness exerts a profound effect on the performance of the device.

An examination of variation of different parameters in relation to the absorber layer's thickness empowers us to engineer a solar cell that achieves exceptional performance. To scrutinize these variations, thicknesses were varied from 0.2µm to 4.0µm. An increment in it leads to a reduction in the open-circuit potential difference (V_{oc}), as evidenced in Figure 4(a).

The observation indicates that at a thickness of 0.2µm, the V_{oc} is measured at 1.375V but significantly diminishes to 1.275V at 4µm. This decline in open-circuit voltage is attributed to the decreased mobility of charge carriers. Figure 4(b) depicts an increasing trend in short-circuit current (I_{sc}) with thickness ranges from 0.2µm to 4.0µm and eventually saturates at around 31.5mA at 2.0µm. At a thickness of 1.0µm, the efficiency reaches its peak at 34.63% but gradually diminishes to its lowest value of 33.7% at 4.0µm.

The fill factor curve depicted in Figure 4(c) exhibits a continuous reduction in its value to 83.41% at 2.0µm. This decline is primarily because of the decrease in open-circuit voltage. Throughout the process, two critical factors, namely carrier mobility and light absorption, govern the device's performance.

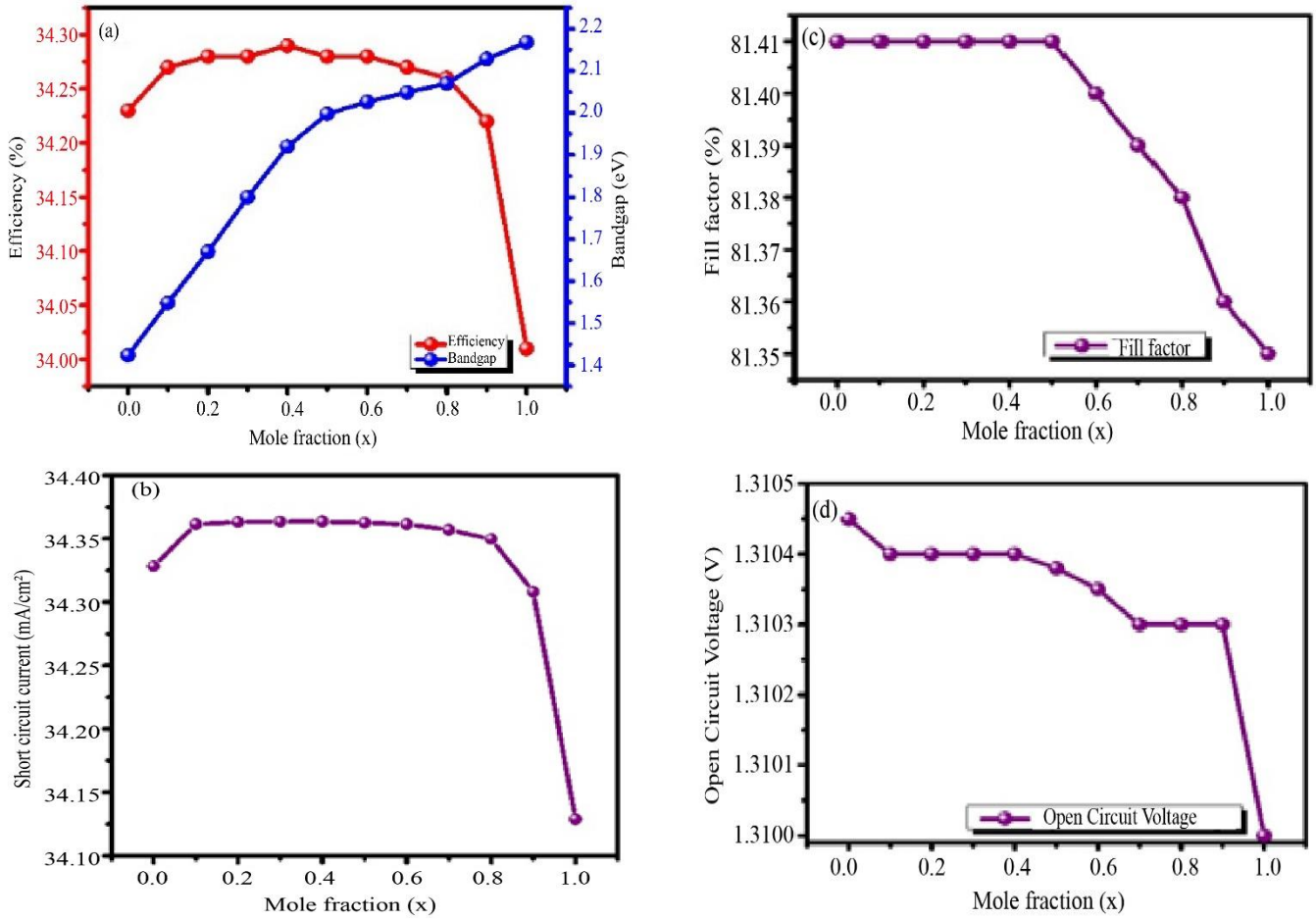

Fig. 2 Influence of composition parameter variation on (a) Band gap, and η, (b) I_{sc}, (c) FF, and (d) V_{oc} for GaAs-based solar cells.

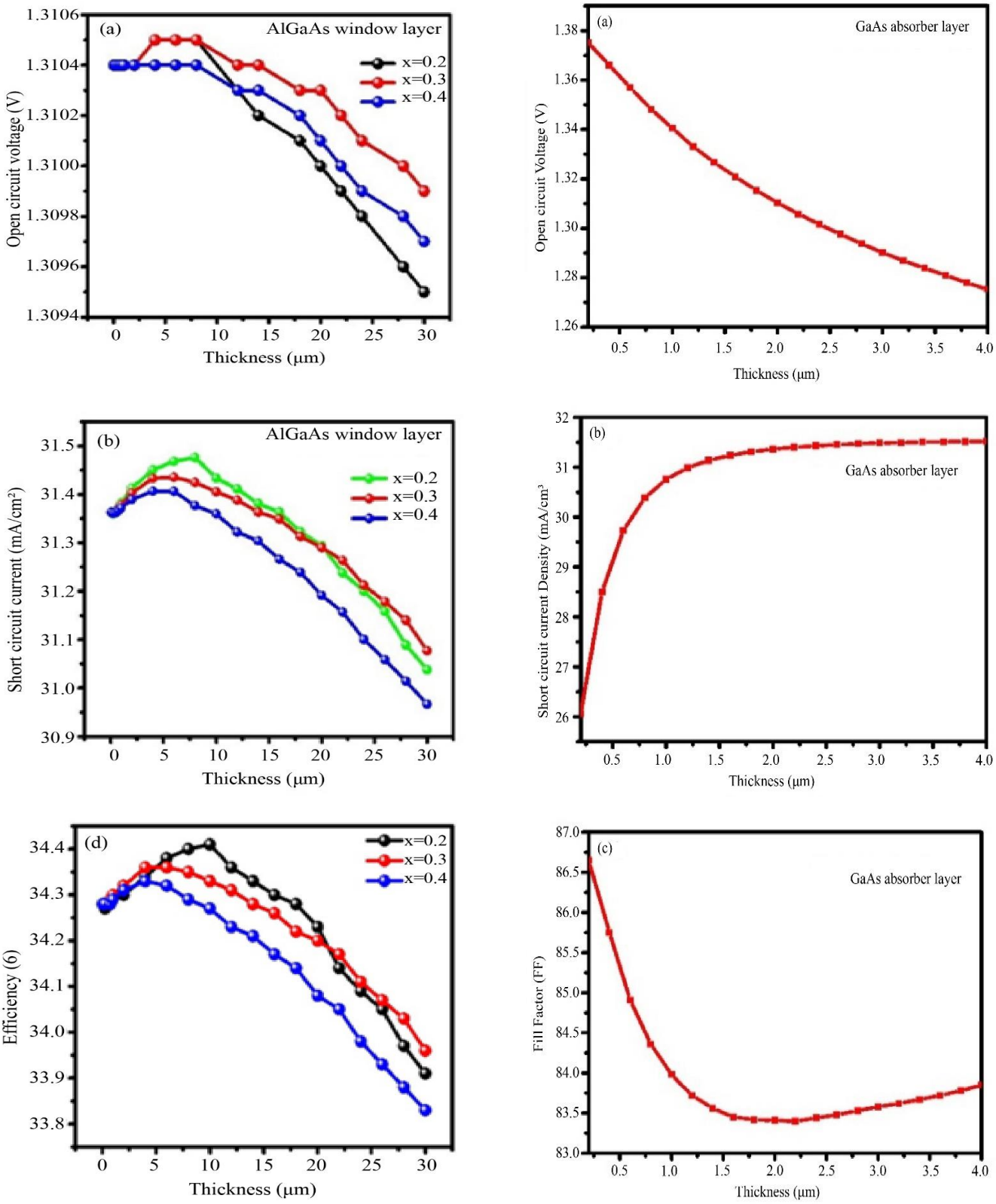

Fig. 3 Optimization of the device parameters (a) V_{oc}, (b) I_{sc}, and (c) η with respect to the window layer thickness.

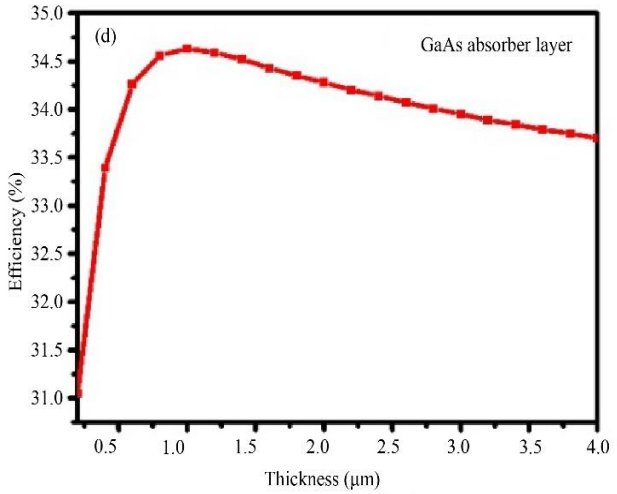

Fig. 4 Absorbing layer thickness effect on (a) V_{oc}, (b) I_{sc}, (c) FF, and (d) Efficiency (η) of the device.

3.2. Thickness Effect of the Back Surface Field (BSF) Layer on the Device

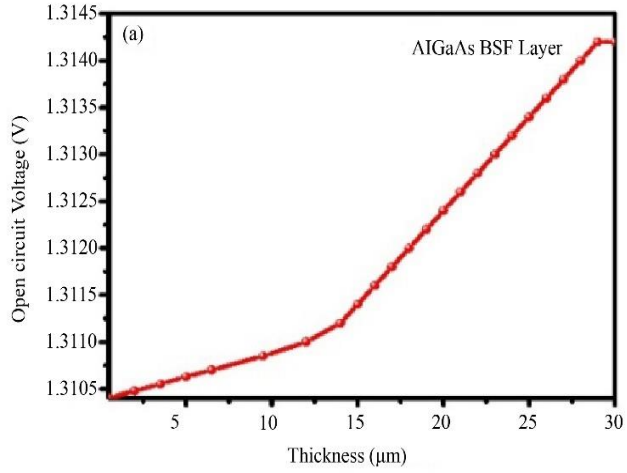

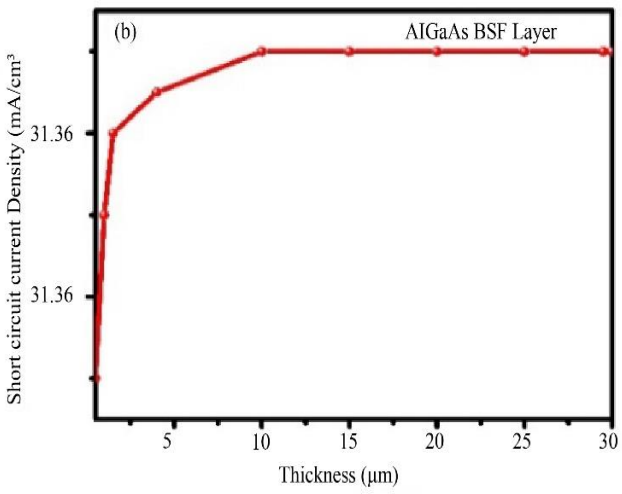

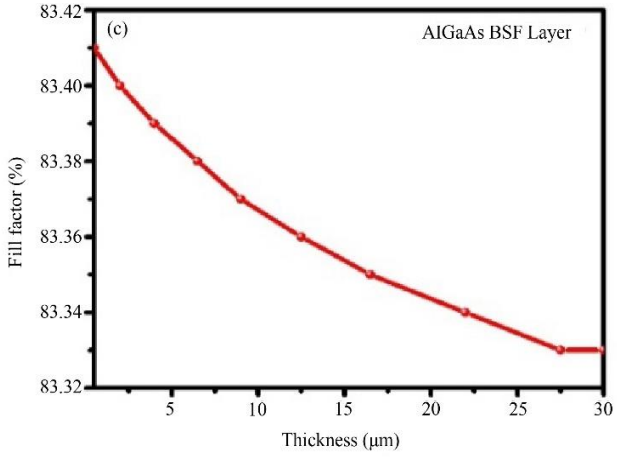

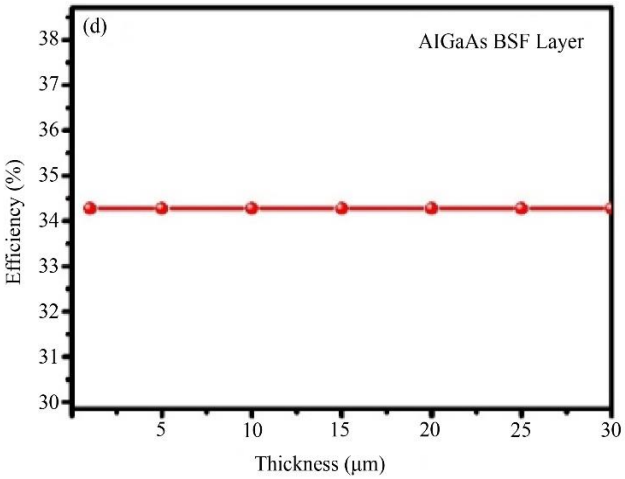

Fig. 5 Optimization impact of back surface field layer on (a) Voc, (b) I_{sc}, (c) FF, and (d) Efficiency (η).

The device's efficiency is contingent upon the effectiveness of its BSF layer. The primary objective of the BSF layer is to facilitate the confinement of photo-generated carriers within the confines of the p/n junction while concurrently avoiding any increase in the device's series resistance. Additionally, the BSF layer exhibits a property known as "photo confinement". The major step in this process involves determining the optimal thickness to examine the key parameters such as I_{sc}, V_{oc}, and overall efficiency (η). Figure 5(a) depicts the variation of the voltage due to an open circuit with an increase in thickness. The voltage reaches a saturation point at 25μm. This phenomenon is because of the BSF layer's role in mitigating charge carrier recombination. A thicker BSF layer contributes to a reduction in recombination at the surface, thereby resulting in an elevation of the potential difference. In tandem with the voltage due to open-circuit, the current due to the short circuit also experiences an increase, which subsequently becomes stabilized. This behavior underscores a trade-off in the fill factor, as evident in Figure 5(c). Remarkably, despite the variations in BSF layer thickness, the overall efficiency, as portrayed in Figure 5(d),

remains relatively constant. The observation suggests that alterations in the BSF layer's thickness have a limited impact on the efficiency.

3.3. Effect of the Carrier Concentration

Figure 6 represents the effect of absorber layer carrier concentration on device characteristics. Elevated carrier concentrations generally yield heightened photon absorption capabilities. The carrier concentration is systematically varied, ranging from $1x10^{10}cm^{-3}$ to $5x10^{17}cm^{-3}$. Figure 6(a) exhibits a constant feature of open circuit voltage up to a concentration of $1x10^{14}cm^{-3}$, then a subsequent decline to a value of 1.3102V. However, with an increase in carrier concentration, an influx of impurities infiltrates the material, engendering energy levels within the band gap. These newly created energy levels serve as recombination centres for charge carriers, thereby curtailing their lifetime within the material. Consequently, this factor reduces open-circuit voltage (V_{oc}).

Figure 6(b) portrays a variation of the short-circuit current (I_{sc}) concerning carrier concentration. Initially I_{sc} remains consistent with the rising doping concentration, then increases with further increment in concentration. This increase in current is because of the electron-hole pair generation and a commensurate reduction in carrier recombination. Figure 6(c) illustrates the fill factor's behaviour in relation to the carrier concentration. The fill factor remains relatively stable, with a minor uptick in carrier concentration.

This stability can be attributed to the presence of a predominantly stable dominant recombination mechanism and a consistent carrier transport process. Figure 6(d) underscores that the solar cell's efficiency remains invariant at lower doping concentrations but experiences an upswing as carrier concentration increases. The solar cell's efficiency reaches an optimal value of 37.03% at a concentration of $5x10^{17}cm^{-3}$. Beyond this threshold, efficiency experiences a decline due to the exacerbation of recombination rates.

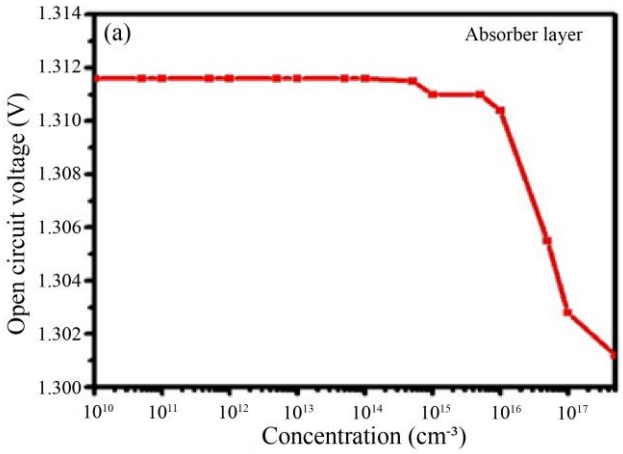

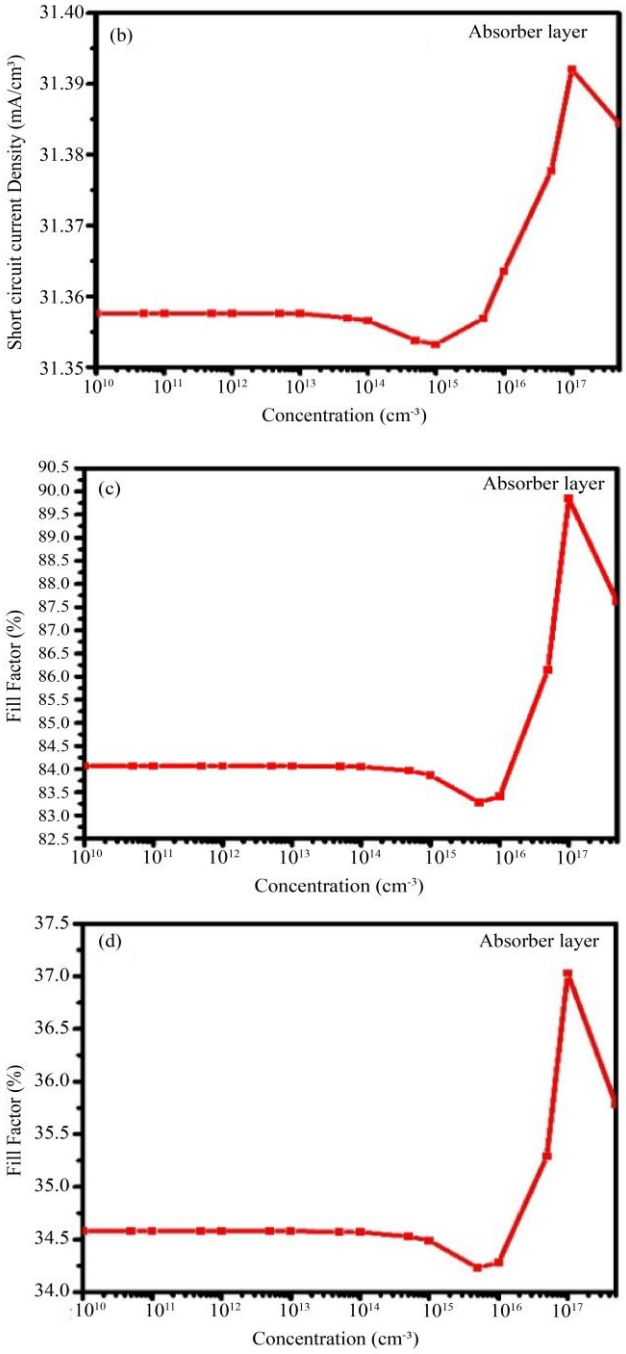

Fig. 6 Absorber layer thickness optimization with regard to various parameters: (a) V_{oc}, (b) I_{sc}, (c) FF, and (d) Efficiency (η).

The application of a p^+-GaAs layer serves to capture minority carriers generated near the solar cell junction, thereby enhancing the collection efficiency. This improvement in carrier collection efficiency translates into a more efficient conversion of incident photons into electrical energy. The broader bandgap of the p^+-GaAs layer allows to absorption of high-energy photons, resulting in effective utilization of the solar radiation and consequently increasing the overall efficiency. Its effect on the electrical properties of

the device is observed in Figures 7(a-d). Figure 7(a) reveals that, as carrier concentration escalates, the open-circuit voltage (V_{oc}) experiences an increase, then saturates to 1.3121V at a concentration of $5x10^{19}cm^{-3}$. This effect in V_{oc} is due to the wider bandgap of the p+-GaAs layer. However, as carrier concentration continues to rise, there is a reduction in carrier diffusion length and an enhancement in the recombination rate. Further increases in carrier concentration do not influence V_{oc} significantly. Figure 7(d) illustrates that the power conversion efficiency escalates with increasing carrier concentration. This elevated efficiency guides to a concurrent rise in the current, as demonstrated in Figure 7(b). Adjacent to the p+-GaAs layer, a Back-Surface Field (BSF) layer exists, accompanied by an electric field that segregates electron-hole pairs. This electric field serves as a driving force for electrons and holes to direct them towards the n-type region and p-type region. Higher carrier concentrations enhance the likelihood of carriers being collected before experiencing recombination, resulting in an amplified short-circuit current. A decreasing fill factor is shown in Figure 7(c) as the carrier concentration rises. This upswing in carrier concentration within the GaAs layer tends to induce more recombination events, auger recombination effects, elevated series resistance, and the emergence of shunt paths. Collectively, these factors contribute to the decrease of the fill factor.

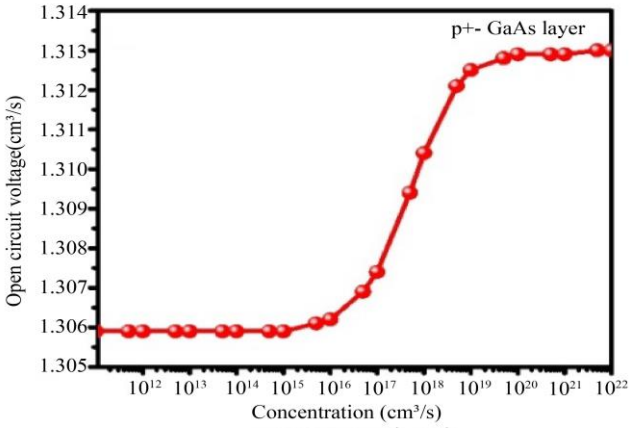

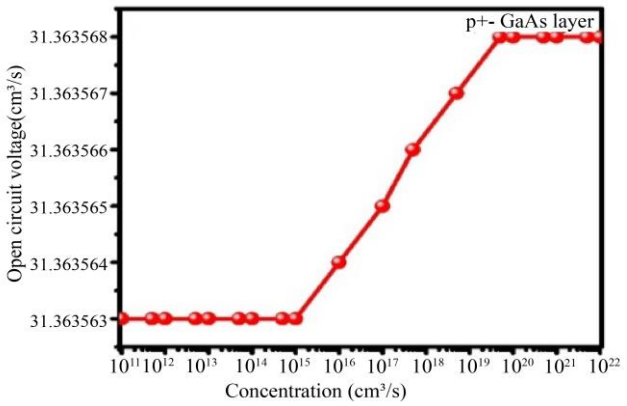

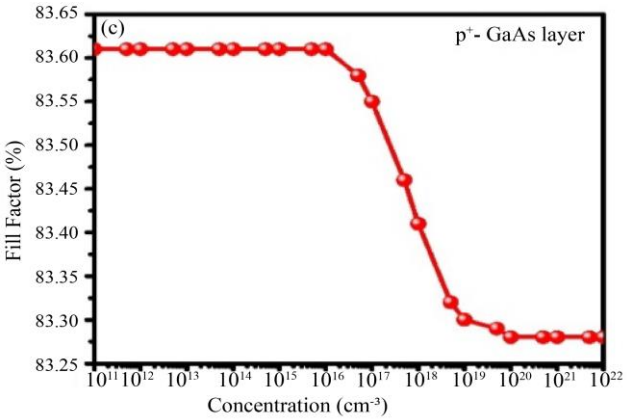

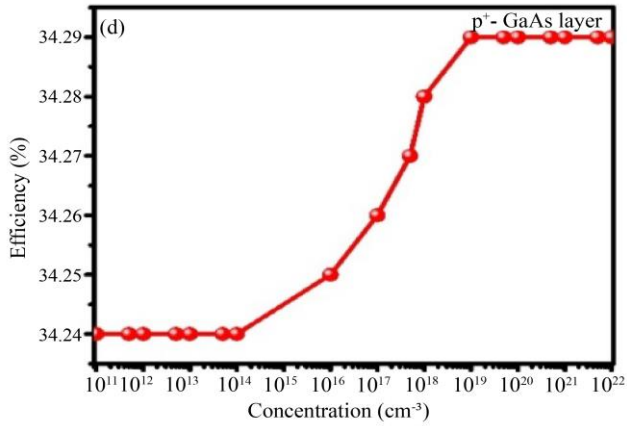

Fig. 7 p+- GaAs layer thickness Optimization with regard to (a) V_{oc}, (b) I_{sc}, (c) FF, and (d) Efficiency (η).

The wide bandgap window layer allows sunlight to effectively penetrate and reach the active region of the solar cell, thereby facilitating efficient electrical conduction. Consequently, the AlGaAs window layer exerts a substantial influence on the device's optical, electrical, and structural characteristics. Notably, variations in the carrier concentration within this layer provide a significant effect on the proposed device as shown in Figures 8(a-d). In Figure 8(a), it is apparent that the V_{oc} remains constant at a value of 1.31V despite of increase in carrier concentration of the AlGaAs window layer.

This exploits that carrier concentration within the window layer does not directly affect the open-circuit voltage. The AlGaAs window layer serves as a conduit for incident light, allowing it to reach the active region and facilitating the collection of photo-generated carriers. As carrier concentration increases, more mobile charge carriers become available for collection, which indicates an enhancement in the I_{sc} as shown in Figure 8(b).

According to the plot, the current attains a saturation level and subsequently decreases as the carrier concentration increases. This improvement shows the consequence of the concentration of charge carriers on the material's optical

characteristics. As the carrier concentration rises, more incident light is absorbed within the window layer, owing to its wide bandgap. However, this absorption also results in a reduction in the amount of light reaching the active region, ultimately leading to a decline in the overall short-circuit current.

Notably, at a concentration of $5x10^{19}$ cm^{-3}, Figure 8(b) illustrates a fall in the short-circuit current. Figure 8(c) illustrates that there is a rise in the fill factor because of a rise in carrier concentration within the window layer. This behaviour is attributable to the thin-film nature of the solar cell, where increased carrier concentration enhances optical transmission, reduces contact resistance, and augments charge carrier concentration.

Consequently, the I_{sc} remains stable, and the FF experiences an improvement, culminating in an overall enhancement of the proposed device's performance, as demonstrated in Figure 8(d).

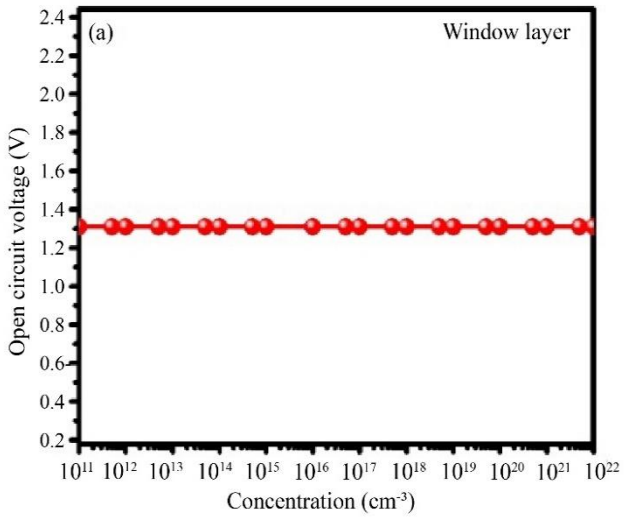

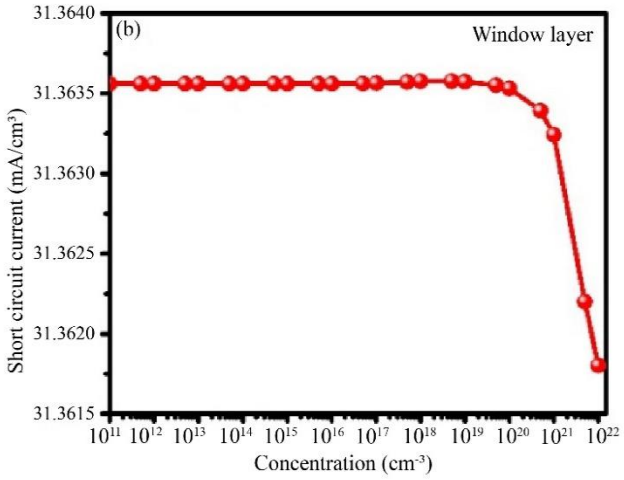

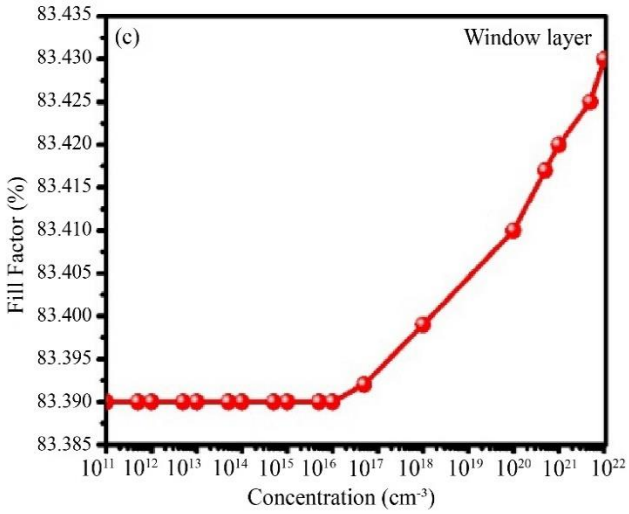

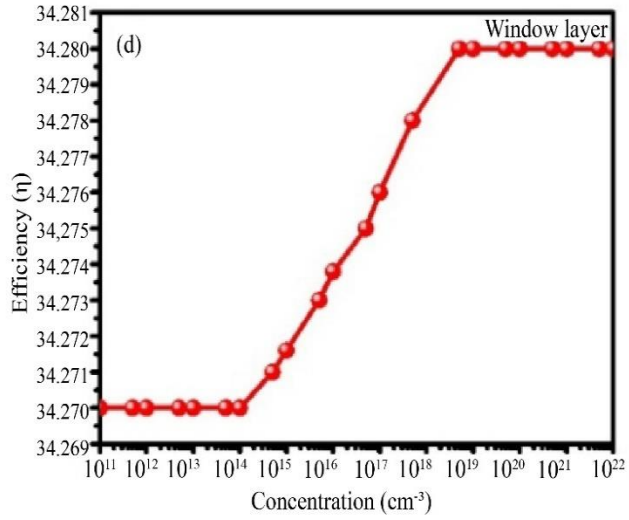

Fig. 8 Window layer carrier concentration optimization with regard to various parameters (a) V_{oc}, (b) I_{sc}, (c) FF, and (d) Efficiency (η) for GaAs-based solar cells

3.4. Effect of the Sun Intensity on Device Parameters

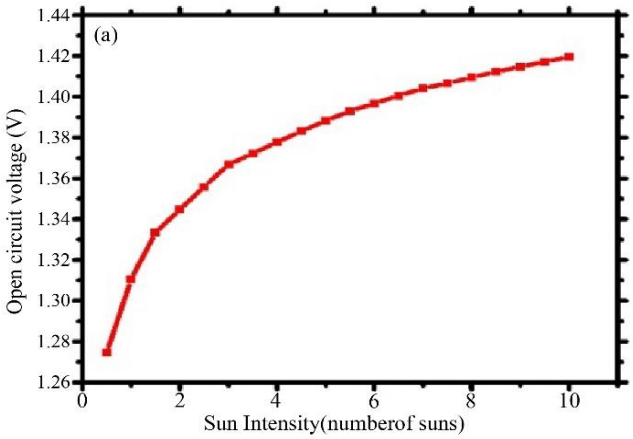

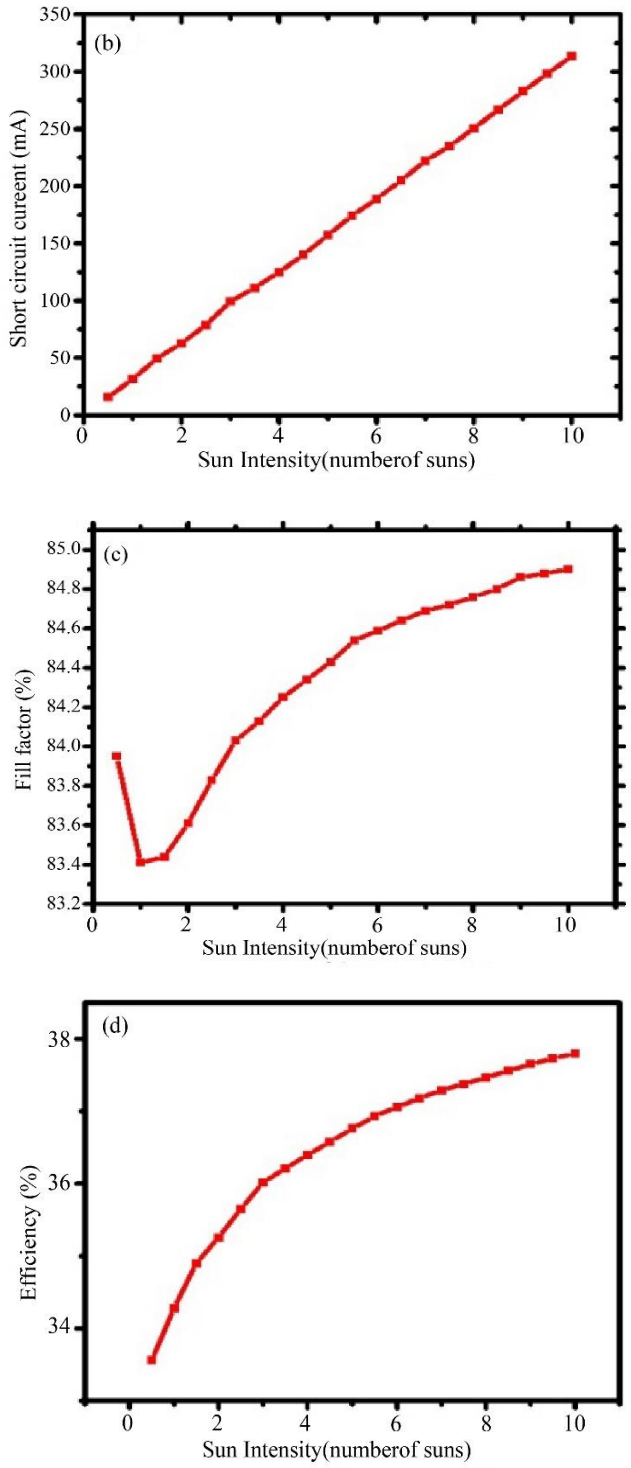

Fig. 9 Electrical parameter variation corresponding to different numbers of suns: (a) V_{oc}, (b) I_{sc}, (c) FF, and (d) Efficiency (η)

Elevated light intensity levels significantly amplify the electrical current generation capability of the structured device, as illustrated in Figure 9(b). The short-circuit current demonstrates a linear relationship with the solar intensity. This is due to a greater photon flux incident upon the device, subsequently leading to a heightened generation of electron-hole pairs. Consequently, the overall power output experiences an increase, accompanied by an improvement in the fill factor and potential difference due to the open circuit. At an intensity level of 10 suns (as depicted in Figure 9(a) and (d)), the open-circuit voltage attains a value of 1.42 eV, coinciding with an impressive efficiency rating of 37.8%.

3.5. Investigation into Radiative Recombination Effects

Radiative recombination affects the efficiency of GaAs photovoltaic cells. Figure 10 represents the effect of radiative recombination. For the purpose of enhancing the cell's performance, it becomes imperative to curtail radiative recombination. In the simulation study, a range of radiative recombination coefficients spanning from 10^{-15} to 10^{-7} cm^3/s was explored. Our findings reveal an optimal range for radiative recombination in the vicinity of $10^{-13}$to 10^{-15} cm^3/s. This range demonstrates the most favourable conditions for achieving peak solar cell efficiency. In the context of the structured device, aimed at realizing enhanced efficiency, it is imperative to minimize both non-radiative recombination and radiative recombination concurrently.

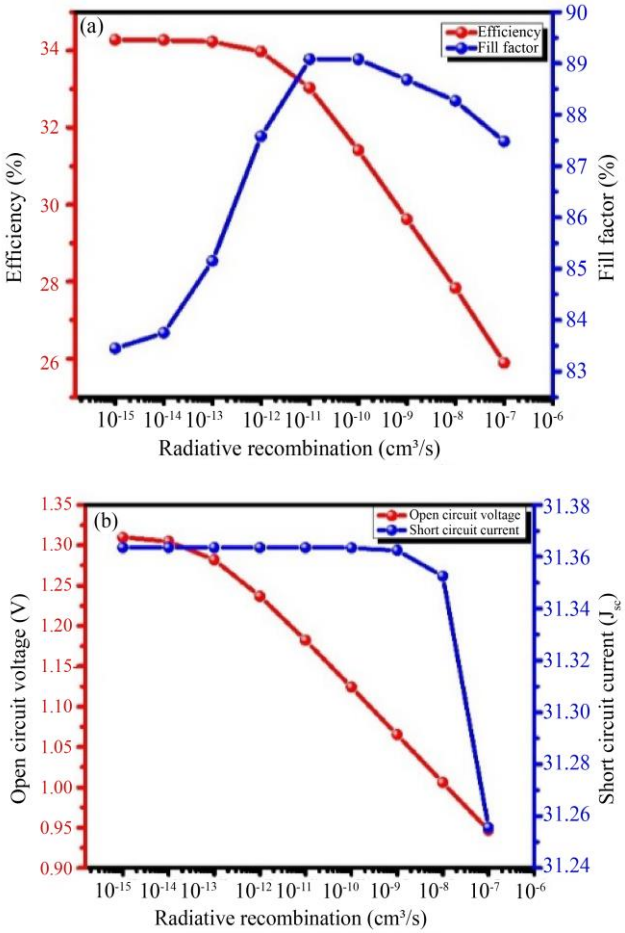

Fig. 10 Effect of radiative recombination on the GaAs solar cell

Table 2. Model validation

Solar Cell Model	Spectrum	Open Circuit Voltage (V_{oc})	Short Circuit Current Density (J_{sc})	Fill Factor (FF)	Conversion Efficiency (η)
Shizhao et al. [10] Type A	AM1.5G	0.857V	24.2mA/cm^2	72.2%	15.0%
Shizhao et al. [10] Type B	AM1.5G	0.862V	25.8mA/cm^2	73.1%	16.3%
Our Model	AM1.5G	1.31V	31.36mA/cm^2	83.41%	34.28%

Table 2 provides a comparison of our model with the previously reported data in Reference [10].

4. Conclusion

This article contains a comprehensive analysis of the impact of mole fraction (x) in AlGaAs, focusing on its analytical implications. Also, it is identified that the optimal composition, with x=0.4, yielded the widest band gap, leading to the highest achievable efficiency. The investigation primarily centered on the enhancement of performance in n+-type AlGaAs window-layered GaAs solar cells, with a specific focus on improving both efficiency and short-circuit current. The assessment of device performance encompassed alterations in thickness, carrier concentration within the window layer, as well as variations in the Back Surface Field (BSF) and buffer layers. Additionally, the device was examined in terms of its susceptibility to radiative recombination. Its findings revealed that the device achieved a remarkable efficiency of 34.28%, a noteworthy improvement compared to single-junction GaAs solar cells documented in prior literature. Consequently, it is evident that meticulous material selection and design optimization collectively contributed to the enhancement of efficiency in GaAs absorber layer-based solar cells.

References

[1] Wen-Wen Zhang et al., "Boosting Photoelectric Performance of Thin Film GaAs Solar Cell Based on Multi-Objective Optimization for Solar Energy Utilization," *Solar Energy*, vol. 230, pp. 1122-1132, 2021. [CrossRef] [Google Scholar] [Publisher Link]

[2] Wenjia Li et al., "Performance Analysis of a Photovoltaic-Thermochemical Hybrid System Prototype," *Applied Energy*, vol. 204, pp. 939-947, 2017. [CrossRef] [Google Scholar] [Publisher Link]

[3] Huaxu Liang et al., "Progress in Full Spectrum Solar Energy Utilization by Spectral Beam Splitting Hybrid PV/T System," *Renewable and Sustainable Energy Reviews*, vol. 141, 2021. [CrossRef] [Google Scholar] [Publisher Link]

[4] Yunyi Ling et al., "A Spectral-Splitting Photovoltaic-Thermochemical System for Energy Storage and Solar Power Generation," *Applied Energy*, vol. 260, 2020. [CrossRef] [Google Scholar] [Publisher Link]

[5] Kirti Saraswat, T. Usmani, and Savita Maurya, "GaAs Solar Cell Performance Improvement by Design Optimization Using NSGA Approach," *Materials Today: Proceedings*, vol. 51, no. 1, pp. 178-185, 2022. [CrossRef] [Google Scholar] [Publisher Link]

[6] Qing Ni, Payam Sabbaghi, and Liping Wang, "Optoelectronic Analysis of Spectrally Selective Nanophotonic Metafilm Cell for Thermophotovoltaic Energy Conversion," *Journal of Quantitative Spectroscopy and Radiative Transfer*, vol. 268, 2021. [CrossRef] [Google Scholar] [Publisher Link]

[7] K.C. Devendra, "Modelling and Simulation of AlGaAs/GaAs Solar Cell," *American Journal of Engineering Research*, vol. 9, no. 4, pp. 218-223, 2020. [Google Scholar] [Publisher Link]

[8] Nikola Papež et al., "Overview of the Current State of Gallium Arsenide-Based Solar Cells," *Materials*, vol. 14, no. 11, pp. 1-16, 2021. [CrossRef] [Google Scholar] [Publisher Link]

[9] Marc Burgelman et al., *SCAPS Manual*, University of Ghent: Ghent, Belgium, pp. 1-155, 2016. [Google Scholar] [Publisher Link]

[10] Nadia Messei, and M.S. Aida, "Numerical Simulation of Front Graded and Fully Graded AlGaAs/GaAs Solar Cell," *Optik*, vol. 126, no. 23, pp. 4432-4435, 2015. [CrossRef] [Google Scholar] [Publisher Link]

[11] Shizhao Fan et al., "16.8%-Efficient n^+/p GaAs Solar Cells on Si with High Short-Circuit Current Density," *IEEE Journal of Photovoltaics*, vol. 9, no. 3, pp. 660-665, 2019. [CrossRef] [Google Scholar] [Publisher Link]

[12] J.K. Arch, and S.J. Fonash, "Using Reverse Bias Currents to Differentiate Between Bulk Degradation and Interfacial Degradation in Hydrogenated Amorphous Silicon p-i-n Structures," *Journal of Applied Physics*, vol. 72, no. 9, pp. 4483-4485, 1992. [CrossRef] [Google Scholar] [Publisher Link]

[13] Tayfun Gokmen, Oki Gunawan, and David B. Mitzi, "Semi-Empirical Device Model for $Cu_2ZnSn(S,Se)_4$ Solar Cells," *Applied Physics Letters*, vol. 105, no. 3, pp. 1-6, 2014. [CrossRef] [Google Scholar] [Publisher Link]

[14] Tobias Kraus et al., "Optoelectronic Simulation of GaAs Solar Cells with Angularly Selective Filters," *Journal of Applied Physics*, vol. 115, no. 5, 2014. [CrossRef] [Google Scholar] [Publisher Link]

[15] L. Zhao et al., "Optimized Resistivity of p-Type Si Substrate for HIT Solar Cell with Al Back Surface Field by Computer Simulation," *Solar Energy*, vol. 83, no. 6, pp. 812-816, 2009. [CrossRef] [Google Scholar] [Publisher Link]

[16] Najmedin Shahverdi et al., "Optimization of Anti-Reflection Layer and Back Contact of Perovskite Solar Cell," *Solar Energy*, vol. 189, pp. 111-119, 2019. [CrossRef] [Google Scholar] [Publisher Link]

[17] M.T. Islam, and A.K. Thakur, "Two Stage Modelling of Solar Photovoltaic Cells Based on Sb_2S_3 Absorber with Three Distinct Buffer Combinations," *Solar Energy*, vol. 202, pp. 304-315, 2020. [CrossRef] [Google Scholar] [Publisher Link]

[18] S.M. Sze, *Physics of Semiconductor Devices*, Wiley, pp. 1-868, 1981. [Google Scholar] [Publisher Link]